Reflectance- and Radiance-Based Methods for the In-Flight Absolute Calibration of Multispectral Sensors

P. N. SLATER, S. F. BIGGAR, R. G. HOLM, R. D. JACKSON, Y. MAO, M. S. MORAN, J. M. PALMER, AND B. YUAN

Optical Sciences Center, University of Arizona, Tucson, Arizona 85721, and U.S. Water Conservation Laboratory, Agricultural Research Service, USDA, Phoenix, Arizona 85040

Variations reported in the in-flight absolute radiometric calibration of the Coastal Zone Color Scanner (CZCS) and the Thematic Mapper (TM) on Landsat 4 are reviewed. At short wavelengths these sensors exhibited a gradual reduction in response, while in the midinfrared the TM showed oscillatory variations, according to the results of TM internal calibration. The methodology and results are presented for five reflectance-based calibrations of the Landsat 5 TM at White Sands, NM, in the period July 1984 to November 1985. These show a $\pm 2.8\%$ standard deviation ($1\ \sigma$) for the six solar-reflective bands. Analysis and preliminary results of a second, independent calibration method based on radiance measurements from a helicopter at White Sands indicate that this is potentially an accurate method for corroborating the results from the reflectance-based method.

Introduction

With the advent of programs designed to monitor long-term changes in land processes, in the environment, and in the global energy balance, the importance of absolute radiometric calibration of satellite-multispectral sensors has come to the fore. The on-board absolute-calibration methods now in use and the precision and accuracy requirements suggested for absolute calibration have been described elsewhere (Slater, 1984; 1985). To summarize, the requirements are that we know the stability of the calibration to a precision of within $\pm 0.5\%$ of the saturation radiance, consistent with the noise-equivalent reflectance difference provided by high-performance sensors, and that the uncertainty in the knowledge of the absolute calibration should be in the range $\pm 1 - \pm 5\%$ depending on the requirements of the scientific investigation for which the calibration is to be used.

In this paper, we review the variations in the in-flight calibration of the Coastal Zone Color Scanner (CZCS) and the Thematic Mapper (TM) on Landsat 4. We then describe the improvements we have made to a reflectance-based method at White Sands, NM, for the in-flight calibration of the TM on Landsat 5. We present results for five absolute calibrations of the solar-reflective bands of TM, and then compare these results with the preflight calibration and with values derived from the TM internal calibrator. We present results of an analysis of a second independent calibration method based on downward-looking ground-radiance measurements from a helicopter. In conclusion we mention future refinements to the reflectance-based technique, including attempts to characterize aerosols more accurately and to account for the adjacency effect and for some of the systematic errors introduced by the sensor's electronics.

52 Vanderbilt Ave., New York, NY 10017 0034-4257/87/$3.50

Variations in Radiometric Calibration

We briefly describe here the variations noted in the calibration of the Nimbus 7 CZCS and the Landsat 4 TM.

With respect to the CZCS, it is worth noting that Gordon (1981), showed that a 5% error in sensor calibration and a 10% uncertainty in the exoatmospheric solar irradiance can combine to give rise to errors exceeding 200% in the retrieval of water reflectance values. Although 10% appears too high for the uncertainty in exoatmospheric irradiance (according to Fröhlich, 1983, it should perhaps be 1–2%), and, although water reflectances are low and therefore relatively hard to measure accurately, the point remains that sensor calibration errors can cause large errors in reflectance measurements. Gordon showed that, by measuring aerosol optical thicknesses and water radiance simultaneously with the satellite measurement of total radiance, one can reduce by an order of magnitude the error in determining water reflectance.

In the summer of 1979, Viollier (1982) compared CZCS-derived water-reflectance values with measurements made near the surface. He found that the satellite value was less than the surface value by 3.5% at 443 nm and greater than the surface value by 6.3 and 12% at 520 and 550 nm, respectively. Viollier comments that, at the 15th CZCS NET Meeting, Gordon reported corresponding values of -2, $+2$, and 7%, but that Gordon had used a different set of calibration constants and exoatmospheric irradiance values.

Gordon et al. (1983a) have described a method for the atmospheric correction of CZCS data that can, in conjunction with ocean reflectance measurements, provide a calibration of the sensor. Their method uses a Monte Carlo atmospheric radiative transfer model and an algorithm that includes a ratio of the aerosol optical depth at wavelengths of 520 and 550 nm to that at 670 nm, where the ocean reflectance is assumed zero. As Aranuvachapun (1983) points out, the accuracy of the algorithm depends mainly on the accuracy of this ratio, which is not currently measured by satellite remote sensing. The uncertainty of the method in determining pigment concentration is stated to be 30–40% over the concentration range 0.08–1.5 $\mathrm{mg\,m^{-3}}$. In three direct comparisons between ship-measured and satellite-determined values of water-radiance, Gordon and associates claim that the atmospheric-correction algorithm had an average error of 10–15%.

By computing the radiance at the satellite from known water-radiance values, Gordon et al. (1983b) proceeded to force agreement between the sensor-recorded radiance and the computed radiance by adjusting the sensor calibration. Their results are shown in Fig. 1 for Band 1 of CZCS. The error bars represent the error induced by the uncertainty in the pigment concentration of the water. Elsewhere in this issue Gordon (1987) addresses the fundamental problems of calibrating CZCS observations.

Hovis et al. (1985) used the second on-board calibration lamp, which is used only occasionally, to check the calibration of CZCS after it had been in orbit for $5\frac{1}{2}$ years. They found no measurable change in the calibration, but it is important to note that the calibration lamp checks only the calibration of the focal plane detectors and associated electronics, as is also the case for the Multispectral Scanner System and the TM. In comparing CZCS data with data from a calibrated radiometer in a high altitude aircraft, Hovis and

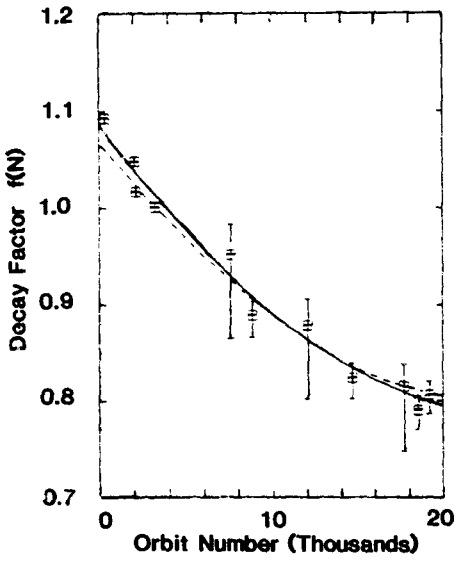

FIGURE 1. The decay factor with orbit number for the first band of the CZCS (Gordon et al., 1983b).

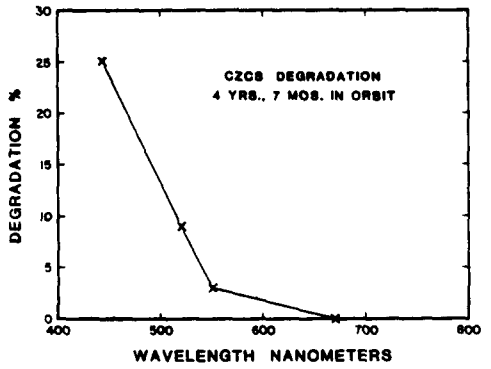

FIGURE 2. The percentage degradation in the response of the CZCS with time for the first four spectral bands (Hovis et al., 1985).

associates found a 25% degradation in the blue band, centered at 443 nm, after CZCS had been in orbit for 4 years and 7 months. The longer wavelength bands exhibited progressively smaller degradations as shown in Fig. 2. Because of the calibration-lamp results, the degradation is attributed to a reduction in the reflectances of the telescope optics and the scanning mirror.

Mueller (1985) has reported on the change in the calibration gains of the first three channels of the CZCS during its first four years of operation. Figure 3 shows the gains for the three channels centered at 443, 520, and 550 nm plotted against year and orbit number. The solid lines are linear regression models and represent the average fits over 20 replications with independent samples of Gaussian random noise. The circles represent decay coefficients calculated for pixels in the central water masses of the northeast Pacific subtropical gyre. The squares are data points generated using the radiometric-sensitivity decay correction models of Gordon et al. (1983b) with random noise, and the dashed lines are their models. Again the tendencies are as noted by the authors cited earlier, although it is interesting to note the linear fit used by Mueller compared to the quadratic fit used by Gordon et al.

Frequently recorded values for the internal-calibrator (IC) gains and offsets for the solar-reflective bands of TM on Landsat 4 have been summarized by Barker (1985a). Figure 4 compares the preflight calibrations with the values from the IC. Again the results, as for the CZCS lamp-based calibration, apply only to changes in the focal-plane filters and detectors and the associated electronics. The graphs in Fig. 4 are divided into three sections. The left section shows the preflight calibration conducted under thermal-vacuum conditions. The middle section shows the results of in-orbit IC calibrations during the so-called Scrounge image-processing era. The third section shows the results during the Thematic Mapper Image Processing System (TIPS) era. The gains G are band averages of 16 detectors derived from the regression equation $P = (G \times E) + O$, where P is

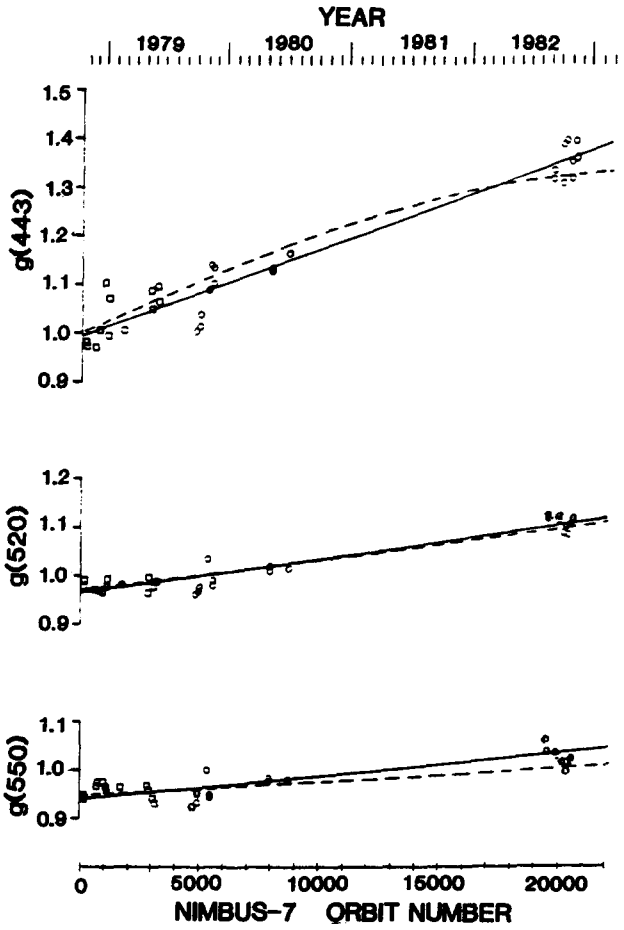

FIGURE 3. Corrections for the radiometric sensitivity of the CZCS with time for the first three spectral bands (Mueller, 1985).

the observed IC pulse, E is the preflight value of the IC "effective" spectral irradiance, and O is the offset.

The results in Fig. 4 show decreases in the apparent gains for Band 1 amounting to 7% and 13% after 500 and 600 days from launch, respectively. Bands 2 and 3 show a similar pattern but with a smaller loss in gain. Band 4 departs from the trend exhibited by Bands 1, 2, and 3 in showing a gain increase for the last calibration. Bands 5 and 7 show oscillatory changes in gain. The amplitude of the oscillations is about 7%. Except for the cyclic pattern in Bands 5 and 7, which are of unknown origin, Barker (1986a) considers most of the changes to be IC-temperature dependent effects and estimates that their magnitude can range between zero and 15% depending on the detector band and IC-flag temperatures at the time of data acquisition. We repeat that, at best, IC-based results are indicative of only changes in the filter-detector-electronics part of the system and that superimposed on them should be the

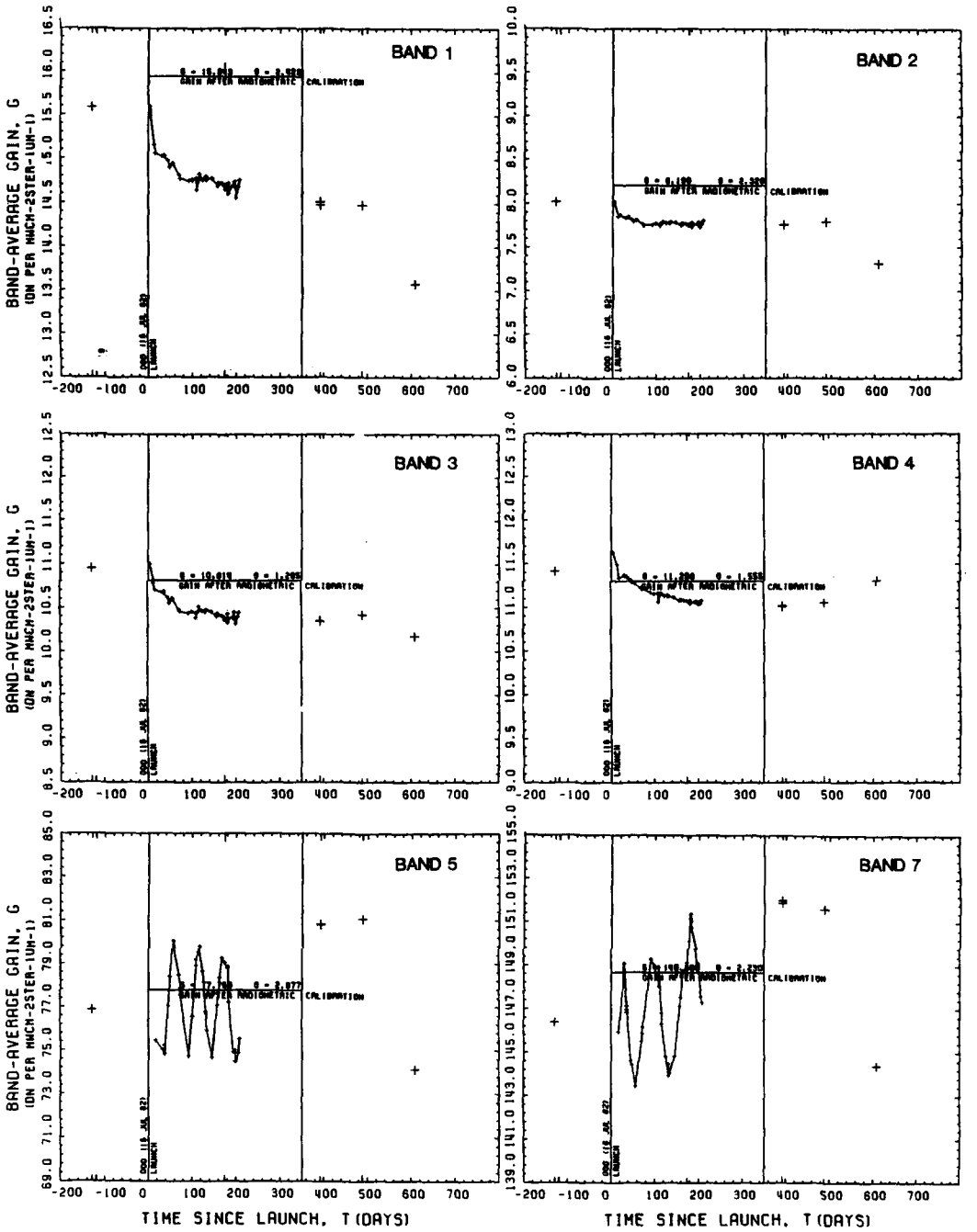

FIGURE 4. The apparent gain change with time for the solar-reflective bands of the TM on Landsat 4. The gain values are in digital counts per $mW\,cm^{-2}\,sr^{-1}\,\mu m^{-1}$ (Barker, 1985a).

changes that occur in the reflectances of the optical components of the telescope and scan mirror.

Reflectance-based calibration of Meteosat

In addition to the work described earlier on the in-flight calibration of the CZCS by reference to known water reflectances, the work of Koepke (1982) on the reflectance-based calibration of Meteosat is noteworthy. He used a radiative transfer program that accounts for multiple scattering in conjunction with ground reflectance data and atmospheric data, to predict the radiance at the entrance pupil of Meteosat I. Atmospheric water vapor was calculated using data from the nearest radiosonde, and the climatological values of ozone and oxygen were assumed. Ground level barometric pressure defined the Rayleigh optical depth, and aerosol optical depths were derived from visibility data. Four test sites were used: rough ocean, the savanna in Namibia, pastureland in northern Germany, and freshly fallen snow. Bidirectional-reflectance data were collected for these sites over a period of several months. Histograms of digital-image counts of these areas typically filled less than three columns, and often one column contained 60% of the pixels. We note, however, that Meteosat quantizes data to 6 bits, so that for low reflectances a three-column spread represents a large variation in reflectance. Nevertheless, by using four targets and pointing the sensor into deep space, which fixed the offset point on the counts-versus-radiance curve, Koepke estimated the uncertainty to be on the order of 6%. This resourceful use of colateral data provided a valuable calibration of Meteosat 1. Koepke's estimate of a 6% uncertainty probably represents a lower limit on the uncertainty of the method because of its dependence on reflectance data that were not collected simultaneously with the Meteosat imagery and because of the use of visibility estimates that provide only approximate values for optical depths.

Reflectance-Based Calibration at White Sands

On 3 January, 1983, we made our first reflectance-based measurements at White Sands, NM, to determine the absolute calibration of the Thematic Mapper on Landsat 4 (Castle et al., 1984; Kastner, 1985). Since then we have made five more sets of measurements for the TM on Landsat 5. During this period we have made improvements with respect to 1) site location, 2) instrumentation, 3) measurement methodology, particularly the measurement of absolute spectral reflectance factor, and 4) data reduction and presentation. These and related topics will be discussed below.

Site location

The alkali flats region at White Sands Missile Range was chosen for reflectance-based calibration purposes because it is a flat, extended area and, in the visible and near infrared, is of high, uniform reflectance. In addition, it is close to being a Lambertian reflector, and it is at an elevation of about 1200 m in a region where the atmospheric aerosol loading is low and the expectancy of clear weather is high.

We require a flat surface to avoid topographically induced variations in radiance across the site. Its being situated near the middle of a high reflectance area about 30×30 km in extent results in the atmo-

spheric adjacency effect (Pearce, 1977) being negligible except in Band 1. Santer (1986), using the "5-S" atmospheric program of Tanré et al. (1985) estimates that the adjacency effect causes our predicted radiance values to be about 1% too high in TM Band 1; the percentage decreases as the wavelength increases. High reflectance and site elevation as well as low aerosol loading reduce the uncertainty in the calibration associated with characterizing the aerosols present (see the later discussion of results). A near-Lambertian surface minimizes the errors introduced by the change in the solar zenith and azimuth angles during the roughly 45 min required to measure the reflectance of our 480×120 m site.

The location for our first measurements on 3 January 1983 was Cherry Site near the southern end of the Northrup strip. We subsequently moved 2 miles east to Chuck Site where we occupy a building serviced by telephone and electricity. It is near a 90° turn in a compacted gypsum road that is detectable on a contrast-stretched TM image; this greatly facilitates the location of our measurement area on the image. Another advantage of Chuck Site is that it is 2–3 m higher in elevation than Cherry Site and many other areas of the alkali flats region of White Sands. We have noticed that these lower lying areas are flooded after heavy rains, sometimes to a depth of 20–30 cm, while the area around Chuck Site is not.

New instrumentation

In this section we briefly describe the design and operation of a new spectropolarimeter, two models of which exist, one can be mounted on a helicopter and the other is attached to an autotracking mount, also described. Both instruments provide polarization data within spectral intervals of 10 or 20 nm. They can cover a 1°, 2°, or 5° field of view and have a dynamic range of 10^4 by use of neutral density filters. A lap-top computer is used for data collection and storage purposes. The spectropolarimeter attached to the autotracking mount is principally used as a solar radiometer, although the tracking mount can also be programmed to provide sky scans. The solar radiometer has the capability, using an Si and a PbS detector, of making measurements from the 0.42 to 2.5 μm. The automatic-tracking capability provides more accurately timed data than can be obtained using a manually operated instrument. The helicopter instrument at present operates only over the range 0.44–1.04 μm; in other respects, the spectropolarimeters are identical.

Each instrument weighs 11 kg, measures $19 \times 26 \times 28$ cm, and requires 10–12 W to operate. A field stop at the focus of the objective lens of each instrument defines its angular field of view and a field lens forms an image of the aperture of the objective lens onto the detector. The position of the filter and aperture wheels, polarizer, wave plate, and detector assembly are computer-controlled with precision placement and monitoring performed by a combination of stepper motors and encoders.

A silicon photodiode detector, Model UV444-B from EG&G, was chosen for the visible and near IR (0.4–1.1 μm) because of its ruggedness and linearity over a large dynamic range. A PbS detector Model #2309 from IR Industries was chosen for the range 1–2.5 μm. The detectors are mounted in a machined slide

allowing both detectors to use the same optics. The detector slide is heated to a stable temperature of about 50°C. The thermal drift is low enough to give a useful signal-to-noise ratio in the IR. However, the ground radiance is too low for the use of an uncooled IR detector in the helicopter instrument.

In the solar instrument, 10 narrowband filters were selected to assist in the characterization of atmospheric constituents in the 0.4–1.04 μm range. Five narrowband filters with central wavelengths in atmospheric windows are used to determine the aerosol optical depth. Three filters in the Chappuis band and one in the water-vapor band are used to determine the extinction due to ozone and water vapor. Three additional filters are provided to cover the IR, two at the band centers of TM bands 5 and 7 and one narrowband filter centered at 2.25 μm.

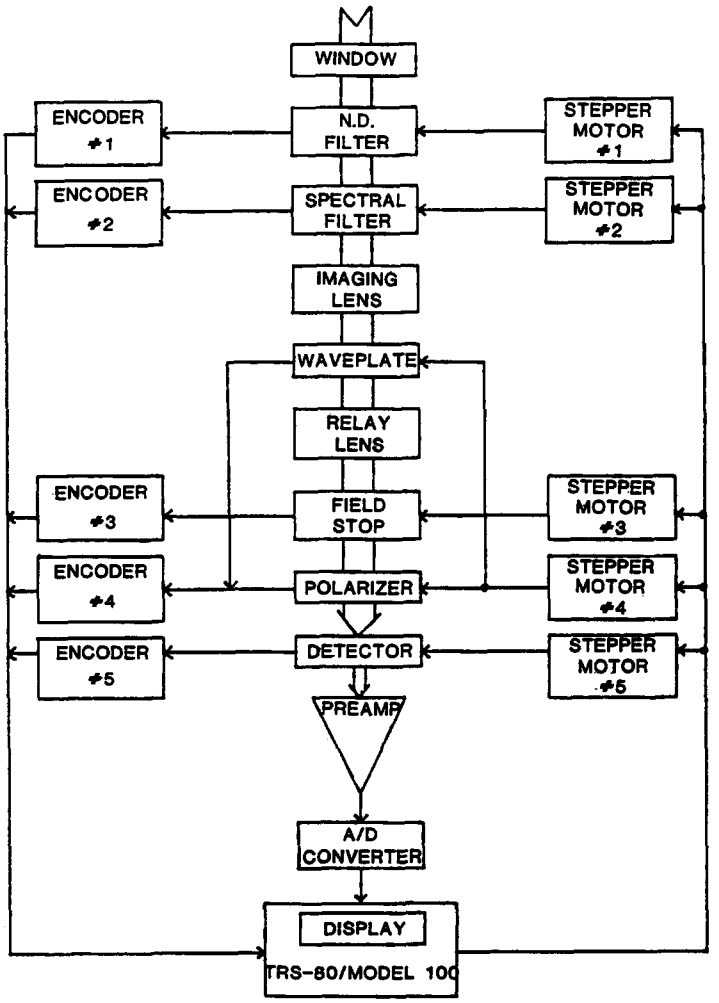

FIGURE 5. Schematic of the optical, mechanical, and electronic components of the spectropolarimeter (Castle, 1985).

The portable spectropolarimeter used in the helicopter for measurements of the site from 3000 m above mean sea level (MSL) contains filters that closely match those in the first four TM bands. In addition, there are eight narrowband filters identical to those used in the solar instrument.

Figure 5 is a schematic of the optical, mechanical, and electronic components of the spectropolarimeter. Light enters the instrument through a protective window, then through neutral density and spectral filters, and then through the objective lens, quarterwave plate, field lens, field stop, polarizer, to the detector. The instrument cycles through the spectral filters, taking two polarization measurements for each filter (the measurements are simply averaged when the spectropolarimeter is used as a solar radiometer). When cycling through the IR filters, the PbS detector is moved into position, and the Si detector is moved out. The detector signal is amplified and then digitized by a 12-bit A/D converter. If the signal is out of range of the A/D converter, the appropriate neutral density filter is moved into position and a new reading is taken. The data are stored on a Radio Shack, TRS 80 Model-100 portable computer for later analysis.

The computer controls the operation of the instrument and acquires and stores the data. The positioning of each component is controlled by stepper motors. The positions of the components are continually monitored through a set of 2-, 3-, or 4-bit encoders. The time is accurately recorded for each data point by reference to the internal clock of the Model 100.

When the instrument is used as a solar radiometer, pointing accuracy and temporal resolution of the data are maintained by an automated elevation-azimuth tracking mount. The mount consists of a tripod, a control box, and two turntables and a yoke. The control box contains power supplies and control interface electronics for the spectropolarimeter and the tracking turntables. The radiometer is moved in azimuth and elevation by two stepper-motor-powered precision turntables. The position of each turntable is monitored by two 12-bit, absolute-position rotary encoders. The computer calculates the sun's position and sends appropriate commands to correct the positions of the turntables. The solar tracking is updated every 30 s and, typically, a complete data set of 12 spectral bands is taken every 3 min.

As expected, the maximum elevation error for the tracker (0.35°) occurs when there is maximum solar change in elevation. Similarly, the maximum error for azimuth, (0.5°) occurs close to noon when there is a maximum change in azimuth angle.

The results of a laboratory experiment have shown that a pointing error of $\pm 0.8°$ for a 2° field of view and $\pm 2°$ for a 5° field of view do not introduce a significant change in the output of the spectropolarimeter. The accuracy of the tracker program is then adequate for our purposes.

The solar instrument, although attached to a heavy tripod and control box, is portable and can be set up easily in nearly all remote field sites so long as 115 V AC power is available. The helicopter instrument is battery operated and is more portable, requiring only a 5 kg battery-interface box and a lap-top computer. It can be attached to a mount on a helicopter, or to a yoke for field measurements.

Ground-based, reflectance-factor measurements

Reflectance-factor measurements of the gypsum sand at White Sands, NM were made using two commercially available radiometers specifically designed for ground-based reflectance measurements in support of satellite experiments. The first, a Barnes Modular Multispectral 8-channel Radiometer[1] (Robinson et al., 1979), nominally duplicates the six TM solar reflective bands. An MMR band without a counterpart on the TM (1.15–1.3 μm) will not be discussed here. The second instrument, an Exotech Model 100-AX, nominally duplicates the first four TM bands. We devised a backpack transport system to suspend a radiometer about 1 m to the right side and slightly above the operator's shoulder level. This system (known as "yoke" or "wings") allows numerous measurements to be made rapidly over an extensive ground area without the need for vehicles. Data were recorded with portable acquisition systems mounted on the front of the backpack system within easy sight and reach.

The absolute reflectances of the gypsum sand targets were estimated by reference to $BaSO_4$ panels. The panels used were constructed by Che Nianzeng at the Optical Sciences Center and calibrated using the field method of Jackson et al. (1987).

Four 16-pixel areas (each pixel representing 30×30 m) were aligned parallel to the track of Landsat 5 at the Chuck Site. The layout of the sampled area is shown in Figure 6. The measurement sequence for the MMR began at the southeast pixel (nearest the block house at the Chuck Site). First, a set of 12 readings was made over the $BaSO_4$ reference panel, then 12 readings about 2 m apart were made on each of the four southernmost pixels, returning to the east on the four pixels immediately adjacent to the north, returning west on the next set of four, and again east on the fourth set of four. The path was north–south centered on each pixel (the MMR readings are diagramed as open circles in Fig. 6). Following the first 16-pixel set, another 12 readings were taken on the $BaSO_4$ reference panel, and the next 16-pixel set was taken. Panel readings were taken after each 16-pixel set.

The Exotech measurement path was east–west centered on the pixels (depicted as dots in Fig. 6). As with the MMR, 12 reference-panel readings were taken first, then the southwesternmost pixel, proceeding 4 pixels north, then back south in the 4 pixels immediately east. The 16-pixel set was completed on the southeasternmost pixel. Panel readings were made after each 16-pixel set. Approximately 45 min were required to record 64 pixels with 24 readings per pixel. The time was centered on the satellite overpass time.

The above-described measurement sequence was followed for 28 August 1985 and 16 November 1985. For 24 May 1985, only the MMR was used (open circles in Fig. 6). On 8 July 1984, and 28 October 1984, only the first 16-pixel set was measured, and only with the MMR.

Reflectance-factor calculations

Reflectance factors were obtained by ratioing the voltage measured over a target to the voltage measured over a

[1] Trade names and company names are included for the convenience of the reader and imply no endorsement of the product or company by the University of Arizona or the United States Department of Agriculture.

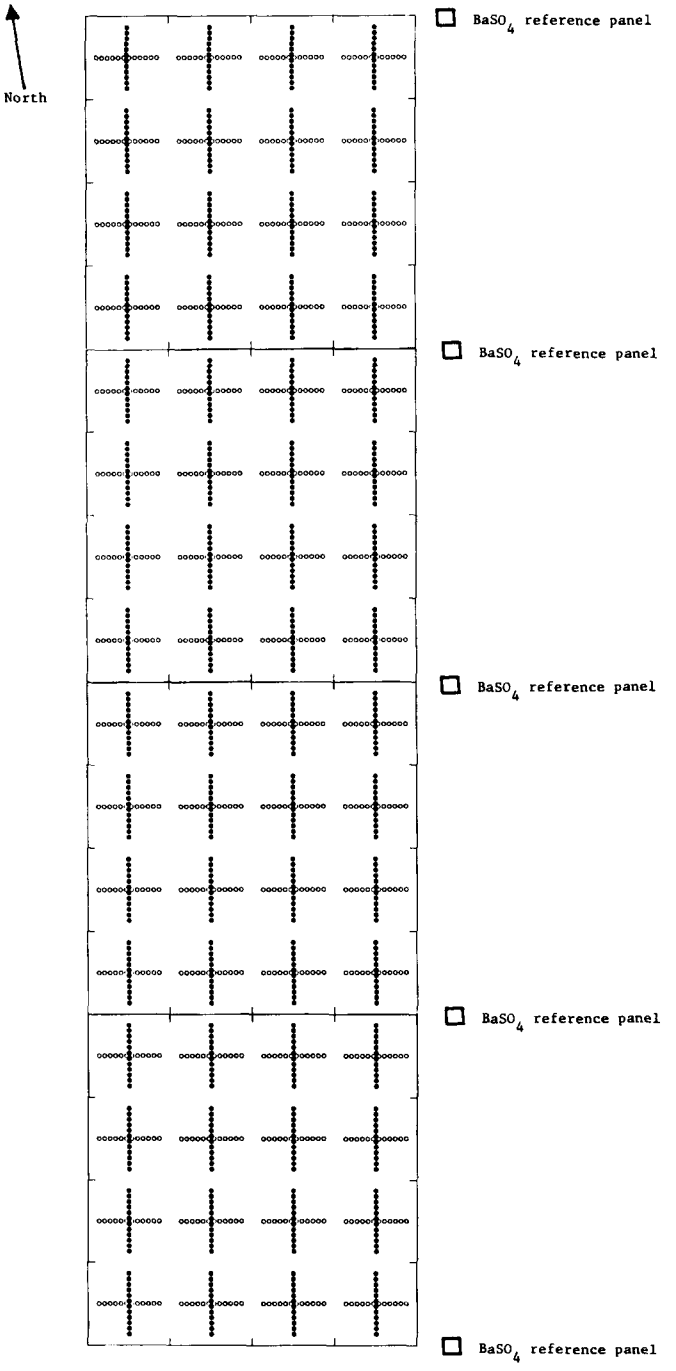

FIGURE 6. The layout of the 16×4 pixel measurement area near Chuck Site on White Sands Missile Range.

TABLE 1 Reflectance Factors for the Four 16-pixel Areas[a]

28 August 1985						
	Equivalent TM Band from MMR					
	1	2	3	4	5	7
D	0.503	0.567	0.610	0.634	0.420	0.115
C	0.503	0.565	0.607	0.627	0.421	0.159
B	0.484	0.543	0.582	0.605	0.407	0.157
A	0.479	0.539	0.580	0.599	0.408	0.163
Average	0.492	0.553	0.595	0.616	0.414	0.159
	Equivalent TM Band from Exotech					
	1	2	3	4		
D	0.507	0.577	0.616	0.649		
C	0.501	0.567	0.605	0.637		
B	0.487	0.548	0.585	0.616		
A	0.478	0.540	0.578	0.607		
Average	0.493	0.558	0.596	0.627		
16 November 1985						
	Equivalent TM Band from MMR					
	1	2	3	4	5	7
D	0.432	0.499	0.539	0.566	0.359	0.128
C	0.398	0.460	0.498	0.527	0.324	0.107
B	0.390	0.450	0.487	0.514	0.306	0.096
A	0.403	0.465	0.502	0.530	0.328	0.107
Average	0.406	0.468	0.507	0.534	0.329	0.109
	Equivalent TM Band from Exotech					
	1	2	3	4		
D	0.430	0.501	0.541	0.575		
C	0.400	0.468	0.507	0.544		
B	0.386	0.451	0.487	0.522		
A	0.394	0.461	0.496	0.530		
Average	0.402	0.470	0.508	0.543		

[a]A = southernmost;
D = northernmost. Measurements with the MMR were taken in the east–west direction, and measurements with the Exotech were taken in the north–south direction.

$BaSO_4$ reference panel, multiplied by the reflectance factor for the reference panel at the particular solar zenith angle. Although fewer than 10 min elapsed between reference panel readings, the voltages were interpolated to the time of target measurement. Details of the reduction of the field measurements to provide reflectance-factor data appropriate for satellite calibration are described in Jackson et al. (1987).

The 12 measurements for each pixel and for each instrument were averaged to produce a single estimate of the reflectance factor for each pixel (typical standard error = ± 0.005). Next, 16-pixel averages were calculated for each of the four 120×120 m areas. Combining the

TABLE 2 Reflectance Factor Data over Gypsum Sand at Five Solar Zenith Angles, Measured with an Exotech Radiometer over One Target Area

Zenith Angle	Equivalent TM Band			
	1	2	3	4
73.4	0.393	0.463	0.497	0.538
63.1	0.397	0.464	0.501	0.542
55.0	0.396	0.464	0.499	0.542
47.0	0.392	0.461	0.497	0.541
45.1	0.393	0.461	0.499	0.541
34.5	0.388	0.454	0.490	0.528

results from the two instruments yielded 384 measurements for each area, for a total of 1536 measurements over the 120 $\times$480 m area for the first four TM bands. Results of this procedure for two dates are given in Table 1. The data in Table 1 show good agreement between the two radiometers, and indicate the small reflectance differences between the four 16-pixel areas.

Non-Lambertian properties of gypsum sands

Because 40–45 min were required for the reflectance-factor measurements, it was necessary to evaluate the non-Lambertian properties of the gypsum sands to determine whether changes in sun angle during the course of the measurements caused differences in the reflectance factors. On two occasions, reflectance-factor measurements were made of the same target at several sun angles. Data for one day are presented in Table 2. For sun zenith changes from 73.4° to 34.5°, reflectance factors for the first four TM bands changed very little, well within the error of measurement. We conclude that the gypsum sands are essentially Lambertian for nadir measurement and for this range of solar zenith angles. Departure from Lambertian characteristics have been observed with nonnadir angles (Begni et al., 1986).

Comparison of radiometer and TM spectral responses

Band response functions for the two radiometers differ slightly from each other and from those of the TM. Since the purpose of making the measurements was to estimate the reflectance factor pertinent to the TM, it was necessary to examine whether the difference in response functions was significant.

Reflectance spectra were measured at Chuck site on 8 March 1986 by Teillet and Fedosejevs (1986). Reflectance factors for the various bands of the TM, MMR, and Exotech were determined by summing the product of the spectra and the response function for each band of each instrument, and dividing by the integral of the response function over each

TABLE 3 Ratios of the Reflectance Factors for the TM, MMR and Exotech

TM Band	TM/MMR	TM/Exotech
1	0.9938	0.9960
2	1.0096	1.0062
3	0.9987	0.999
4	1.0035	1.008
5	1.0080	—
7	1.0053	—

band. Ratios of the reflectance factors for the TM in relation to the MMR and Exotech are shown in Table 3. The differences are less than 1%.

Numerical procedure for locating site on TM imagery

Reflectance-factor values for the 64 pixels were used in a simple BASIC program to identify the site in the TM data. Reflectance-factor values were converted to approximate digital counts to reduce the effect of rounding errors. A window of TM digital counts (DCs) covering an area encompassing the site was compared, pixel by pixel, to the array of reflectance-factor-based DCs. The standard deviation of the differences between the TM-pixel DCs and the reflectance-factor-based DCs was calculated for the first 64 pixels of the array. Next, the set was moved one column and the new deviation was calculated. The 64-pixel overlay was moved over all columns, then lowered a row, and over all columns again until all pixels in the array had been compared with the reflectance-factor-based DCs. The site was indicated by the position of the overlay having the lowest standard deviation. This procedure quantified the otherwise subjective visual location of subtle differences on the generally uniform white gypsum.

Description of data summary tables

Table 4 lists the results of the TM-5 calibrations at White Sands on 18 October 1984. Tabular summaries for 8 July 1984, 24 May 1985, 28 August 1985, and 16 November 1985, can be found elsewhere (Slater et al., 1986).

The determination of the quantities listed in Table 4 is briefly as follows: The Rayleigh optical depth was determined from a knowledge of the barometric pressure and wavelength. The total optical depths were determined from the slopes of Langley plots in which the log voltages from the solar radiometers were plotted against air masses. In spectral regions unaffected by absorption, the Mie optical depth at any wavelength was determined by subtracting the Rayleigh from the total optical depth at that wavelength. An optical depth vs. wavelength curve was fitted through the points that spanned the absorption region due to ozone. The differences between the values on this curve at a given wavelength and the total minus Rayleigh value at the same wavelength gave the ozone optical depth at that wavelength. A Junge radial size distribution (Junge, 1963) was assumed for the aerosols. The Junge ν parameter is defined in the equation

$$\frac{dN}{dr} = Cr^{-(\nu+1)}$$

where N is the number of particles, r is their radius, and C is a constant. The value of ν, needed to find the aerosol phase function, was determined from the slope of the $\log \tau_{\mathrm{MIE}}$ vs. $\log \lambda$ curve.

A computer program by Dave (1969) was used to determine the scattering phase function and the single scattering albedo. This program is included as one of the subroutines within the Herman code.

The LOWTRAN 6 program by Kneizys et al. (1983) was run to determine the transmittances of water vapor and carbon dioxide in the solar-reflective bands. Average optical depths for water vapor and carbon dioxide ($\tau_{\mathrm{H_2O}}$ and $\tau_{\mathrm{CO_2}}$) were determined for TM bands 4, 5, and

TABLE 4 Calibration of the Thematic Mapper at White Sands on 28 October 1984[a]

THEMATIC MAPPER BANDS	1	2	3	4	5	7
Central wavelength (μm)	0.4863	0.5706	0.6607	0.8382	1.6770	2.2230
τ_{MIE}	0.1360	0.1027	0.0750	0.0401	0.0028	0.0007
τ_{RAY}	0.1420	0.0739	0.0407	0.0156	0.0010	0.0003
τ_{ozone}	0.0047	0.0198	0.0098	0.0011	0.0000	0.0000
Tau water vapor	0.0000	0.0000	0.0000	0.0454	0.1241	0.0805
Tau carbon dioxide	0.0000	0.0000	0.0000	0.0000	0.0094	0.0035
Spectral reflectance	0.4380	0.5006	0.5407	0.5850	0.3592	0.1261
E_0 across band (W/m^2 μm)	1955.5	1826.9	1545.0	1042.8	220.19	74.78
Average image digital counts	222.69	117.19	140.38	119.69	102.50	26.44
Preflight cal gains	15.553	7.860	10.203	10.821	78.751	147.719
Preflight cal offsets	1.8331	1.6896	1.8850	2.2373	3.2905	3.2117
IC cal gains for 28 Oct 84	14.211	7.264	9.551	10.427	76.87	145.004
IC cal offsets for 28 Oct 84	2.2570	2.2160	2.3700	2.3640	3.1400	3.4440
Normalized code radiance	0.0805	0.0870	0.0973	0.0970	0.0491	0.0197
Code TM L (W/m^2 sr μm)	159.60	161.21	152.32	102.56	10.96	1.49
Spectral L from preflight cal	142.00	146.95	135.74	108.54	12.60	1.57
Spectral L from IC cal	155.11	158.28	144.50	112.52	12.93	1.59
% (Code-Pre)/Pre	12.4	9.7	12.2	− 5.5	− 13.0	− 5.0
% (Code-IC)/IC	2.9	1.9	5.4	− 8.9	− 15.2	− 5.8
Counts per unit radiance	1.395	0.727	0.922	1.167	9.351	17.699
Case for Rayleigh Atmosphere						
Normalized code radiance	0.0870	0.0979	0.1055	0.1141	0.0701	0.0246
Code TM L (W/m^2 sr μm)	172.45	181.33	165.20	120.59	15.64	1.87
Counts per unit radiance	1.291	0.646	0.850	0.992	6.553	14.173
Case for No Atmosphere						
Normalized radiance	0.0857	0.0980	0.1058	0.1145	0.0703	0.0247
TM L (W/m^2 sr μm)	169.90	181.41	165.71	121.01	15.69	1.87
Counts per unit radiance	1.311	0.646	0.847	0.989	6.533	14.135

[a]Solar zenith angle Z = 52.068; solar distance in AU = 0.9932; Junge size distribution = 4.09; aerosol size range = 0.02–5.02 μm; refractive index = 1.54–0.01i; time of overpass = 10:09.1 MST; calculated visibility = 120 km; latitude = 32° 55′; longitude = 106° 22′; elevation = 1196 m; pressure = 663.7 mm Hg; temperature = 12.4°C; relative humidity = 75%; nadir viewing angle = 5°.

7 by integrating the LOWTRAN transmittance spectra between the spectral response limits of the TM bands as defined by Palmer (1984). The τ_{H_2O} values were found to be 0.035, 0.0915, and 0.0594, and the τ_{CO_2} values were 0.0, 0.0094, and 0.0035, respectively. The range of predicted τ_{H_2O} values for White Sands was determined by scaling these τ_{H_2O} values by the ratio $\rho_{H_2O}(0, RH, T)/0.59$, where $\rho_{H_2O}(0, RH, T)$ can vary, at White Sands, between 0.01 and 1 g cm^{-2} km^{-1}. The relative humidity and temperature were measured at Chuck Site at the time of overpass. The amount of atmospheric water vapor was then determined from a family of curves of different constant relative humidities that are on a graph of water vapor concentration plotted against temperature (McClatchey et al., 1972).

The normalized code radiances refer to the results of calculations using a radiative transfer code described by Herman and Browning (1975). The radiances are at the entrance pupil of the TM for unity exoatmospheric spectral irradiance. For use in the code, the atmosphere is divided into a sufficient number of plane-parallel layers such that changes within each layer are due only to single-scatter-

ing processes. The Gauss–Seidel iterative technique is used to solve the equation of radiative transfer. Upon convergence, all multiple scattering effects have been taken into account. Values of 5.02, 0.02, and 0.04 μm were used for the maximum and minimum radii and incremental step size, respectively, for the aerosols. A vertical aerosol distribution as measured by Elterman (1966) was assumed. The aerosols were given a refractive index of $1.54-0.01i$, an average value for the region as measured by Jennings et al. (1978). The assumed value for the imaginary part of the index is considered high by Bohren and Hoffman (1983). It is interesting to note that, using a value of $1.54-0.005i$, Kastner (1985) has shown that the radiance at the sensor is 3% higher.

The exoatmospheric spectral irradiance data are those recommended by Fröhlich and published by Iqbal (1983). They represent a carefully edited combination of results published by Neckel and Labs, Thekaekara, Arvesen, and others. The values were adjusted to yield an integrated value of 1367 Wm^{-2}, the solar constant as proposed by the World Radiation Center (see Iqbal, 1983).

The code TM spectral radiance is the product of the exoatmospheric irradiance and the normalized radiance determined from the Herman code.

The average number of image digital counts was determined for the TM image of the site. For the first measurement the site comprised two areas each 4×4 pixels in size on opposite sides of a compacted-gypsum road. For the second measurement the site was 8×4 pixels on the north side of the road, and in the last three cases it was 16×4 pixels, also north of the road. For our calibration of the Landsat 4 TM (Castle et al., 1984), we had to identify the particular detectors crossing the 4×4 pixel area. This is not so important for the Landsat 5 TM because the detector response uniformity is much better. Nevertheless, we did decide to measure the reflectance of an area 16 pixels long in the track direction so as to be taking all detectors into account in the average value used for calibration.

We used data supplied by Barker (1985b and 1986b) to compare our calibration to those obtained preflight and in-flight from the internal calibrator (IC). The relation between average spectral radiance, L_T, and digital counts, DC, is $L_T = (\mathrm{DC} - O)/G$, where G and O are gain and offset. The average values for the gains and offsets of the 16 detectors in each band are listed in Table 4 for all the bands. The absolute calibration is given in counts per unit spectral radiance to provide a value that appropriately decreases with a decrease in the transmittance of the optics or with a reduction in the responsivity of the detectors. A single value is an adequate description of the calibration of the TM because the preflight calibration and IC show the system is extremely linear in its response. Only for low radiance cases, corresponding to less than about 30 DCs, does the system depart from linearity.

The lower two sections of Table 4 are included to compare our results with those computed for a Rayleigh atmosphere and no atmosphere.

Discussion of reflectance-based calibration results

The spectral radiance results in Table 4 for TM Bands 1–4 are graphed in Fig. 7. The abbreviations beneath the figure apply to spectral radiance values as follows: PRE, the values corresponding to

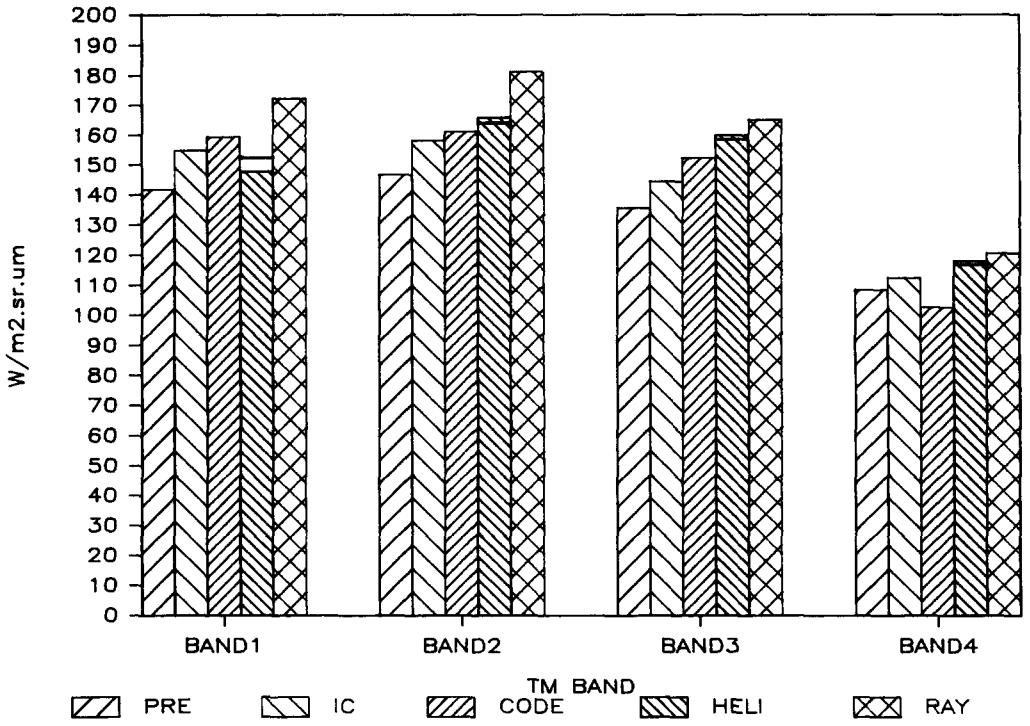

FIGURE 7. The results of the TM calibration of 28 October 1984; see text.

the preflight calibration gains and offsets and the digital counts for the image of the site; IC, the values corresponding to the internal calibrator gains and offsets for that day and the digital counts for the image of the site; CODE, the values as determined from the ground and atmospheric measurements, a knowledge of the exoatmospheric irradiance, and use of Herman's radiative transfer code; HELI, the radiance values measured by the helicopter, where the additional lines at the top of these bars show the helicopter values as corrected by reference to the percentage differences in Fig. 12; and RAY, the values using the same spectral reflectances and exoatmospheric radiances as used in the CODE but assuming a Rayleigh atmosphere.

Several points are noteworthy. First, the CODE and corrected HELI values agree closer with the IC values in Bands 1, 2, and 3 than with the PRE values. Second, the PRE values are always less than the IC and corrected HELI values; Band 4 provides the single exception of the PRE exceeding any other value. This indicates that, on this date, TM had less responsivity than preflight, and, because the IC values generally tend to be lower than the CODE and corrected HELI values, the decrease in response is likely to be due to both a decrease in transmittance of the telescope and a decrease in response of the filter/detector/electronics. Third, the corrected HELI values agree well with the CODE values. This is particularly true for TM Bands 1, 2, and 3. The difference between the CODE and HELI values in Band 4 may be due to a systematic error in the calibration of the helicopter radiometer and/or an er-

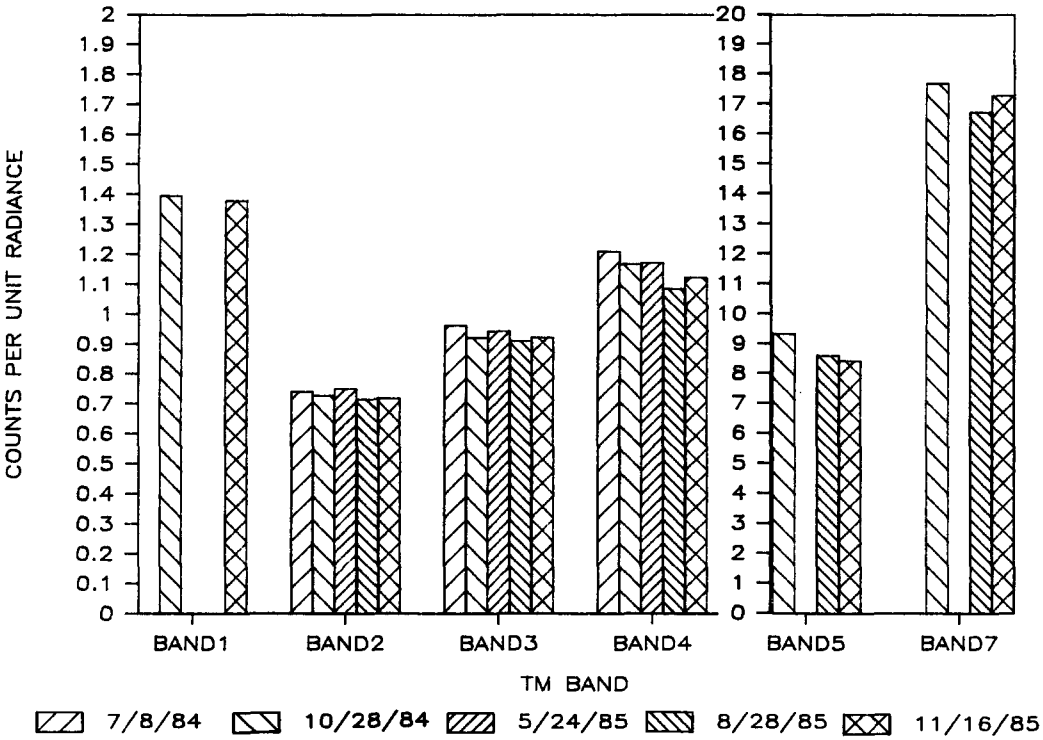

FIGURE 8. The results of TM calibrations at White Sands on five dates over the period July 1984 to November 1985.

ror in the assumptions used in the code, e.g., the Junge ν value or the complex index of refraction of the aerosols, which has been assumed to be wavelength-independent. Finally, in earlier presentations of these data (for example, Biggar et al., 1985), substantial differences were reported between PRE and IC and the CODE, HELI, and RAY values. Recently, these differences have been found to be due to the inadvertent use of an image extraction program that rescaled the image to set the maximum pixel digital count in the image to 255. This gave rise to errors that varied from band to band and that were tentatively explained as being due to luminescence effects in the thin atmosphere that surrounds the spacecraft following an adjustment of the orbit. Fortunately, the present consistent results do not require such an imaginative explanation.

Figure 8 compares the counts per unit radiance for our five measurement dates. It is evident that there is a general tendency for the counts per unit radiance i.e., the system response, to decrease over the 16-month measurement period. In contrast to the results reported earlier for the CZCS, the results do not show a noticeable wavelength dependence.

Figure 9 compares the average values for counts per unit radiance for the five measurements with the average IC-derived values for four dates (no IC data are available for 24 May 1985). There is excellent agreement between the CODE and IC values in the visible and less, but

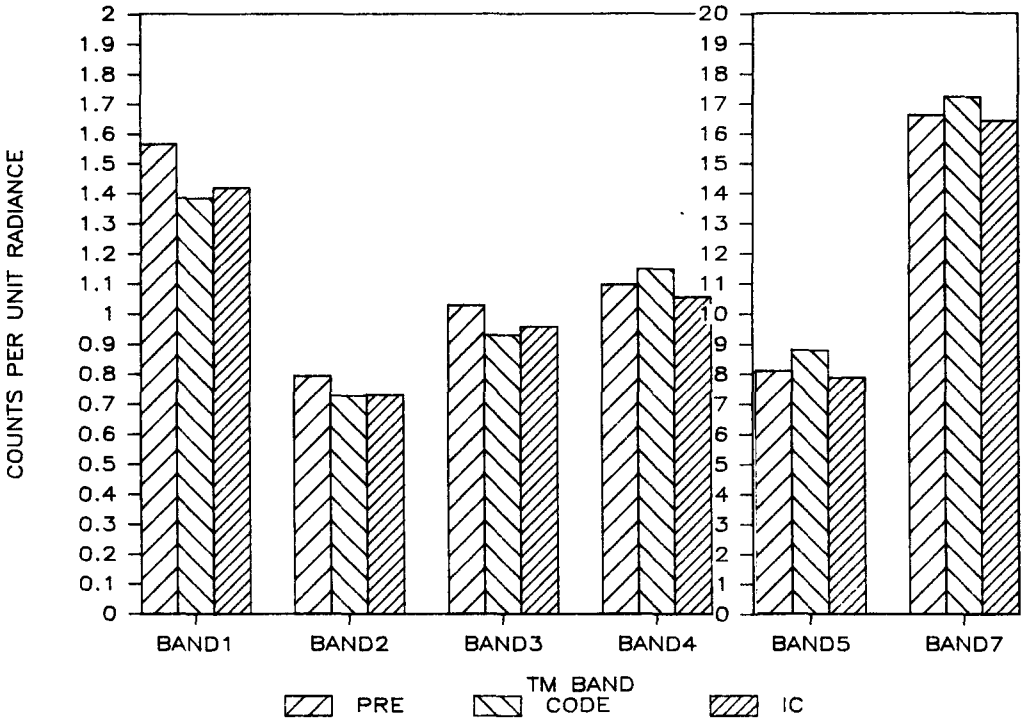

FIGURE 9. The averages of the results in Fig. 8 compared with the average IC values and the preflight calibration.

still good agreement in the IR. The band 5 and 7 comparisons, it should be remembered, are inadequate because only three data sets are involved, and Barker (1986a) has noted that the IC response for the TM-5 may be oscillatory as it was for TM-4 (see Fig. 4).

The results in Table 4 for 28 October 1984 and those for the other four dates (Slater et al., 1986), include results for a Rayleigh atmosphere and no atmosphere. It is interesting that for TM Bands 1–5 and Band 7 the full-atmosphere radiances are 93, 89, 92, 85, 70, and 80% of the radiances for the Rayleigh case, respectively. The small differences between the spectral radiances for the Rayleigh and full atmosphere cases are due to aerosol scattering and absorption. The latter cannot be so accurately determined as the surface spectral reflectance and barometric pressure, which are all that are required as input to a radiative transfer code to determine the spectral radiance at the top of a Rayleigh atmosphere. Thus the major component of the spectral radiance can be determined accurately at White Sands because of its high surface reflectance and elevation and atmospheric visibility. Fortunately, the uncertainties introduced into the final result by the more difficult quantities to determine, for example, aerosol scattering and absorption, have a secondary effect on the final result. Also interesting is the extremely close agreement between the Rayleigh and no-atmosphere results in Table 4. These show that the attenuation

by scattering in the Rayleigh case is almost exactly offset by the path-radiance component incident at the satellite.

Radiance-Based Methods

Figure 7 shows that the radiances as measured at 3000 m MSL at White Sands are about the same as those measured by the TM. This result prompted a more detailed examination of the variation of radiance with altitude as a function of wavelength, reflectance, and visibility.

Starting with the atmospheric conditions of 28 October 1984, at White Sands and with a solar zenith angle of 35°, we calculated radiance values for altitudes between ground level (1196 m at White Sands) and 21,000 m (the operational altitude MSL of the NASA U-2 or ER-2 aircraft) and for above the atmosphere. Graphs were then plotted of the percentage difference (the differences between the radiance above the atmosphere and at an intermediate altitude divided by the radiance above the atmosphere, the whole quantity expressed as a percentage) against MSL. These are shown in Fig. 10 for the first four solar reflective TM bands. As anticipated, the results for reflectances less than 0.1 show large percentage differences, but what is intriguing is the sign change in the percentage difference for reflectances between 0.25 and 1.0 for Bands 1, 2, and 3 and between 0.1 and 0.25 for Band 4. These results show that, for a reflectance of 0.5 and an altitude of 3000 m MSL, the percentage differences are +2.5, −1.0, −1.0, and −2.0 for Bands 1, 2, 3, and 4, respectively. This verifies the experimental observation that for the White Sands conditions of 28 October 1984, helicopter radiance values at an altitude of 3000 m MSL are close to those for space and require only a small correction, which can be made accurately.

With this promising result, the investigation was extended to determine how general this condition might be. Visibilities of 10 and 23 km were considered for a reflectance of 0.5 at all wavelengths. The input values are listed in Table 5, the refractive index was $1.54-0.01i$ in all cases, and Junge ν values of 2.9 and 2.6 were used for the visibilities of 10 and 23 km, respectively.

The output plots of percentage difference, as defined earlier, against altitude above MSL are shown as Figs. 11 and 12 together with the Rayleigh atmosphere curve for a wavelength of 0.49 μm. The positive difference for $\lambda = 0.49$ μm is due to the fact that the large path-radiance term contributed more to the total radiance than is lost by the attenuation of the ground-reflected term. The other curves show increasing nega-

TABLE 5 Input Values for Radiative Transfer Calculations

Wave length (μm)	τ_{RAY}	τ_{O_2}	τ_{H_2O}	τ_{CO_2}	$V = 10$ km τ_{MIE}	$V = 23$ km τ_{MIE}
0.49	0.1630	0.0066	0.0	0.0	0.5393	0.2927
0.57	0.0844	0.0277	0.0	0.0	0.4665	0.2657
0.66	0.0466	0.0136	0.0	0.0	0.4089	0.2434
0.84	0.0178	0.0016	0.0335	0.0	0.3303	0.2111
1.64	0.0011	0.0	0.0915	0.0094	0.1766	0.1391
2.22	0.0004	0.0	0.0594	0.0035	0.1374	0.1176

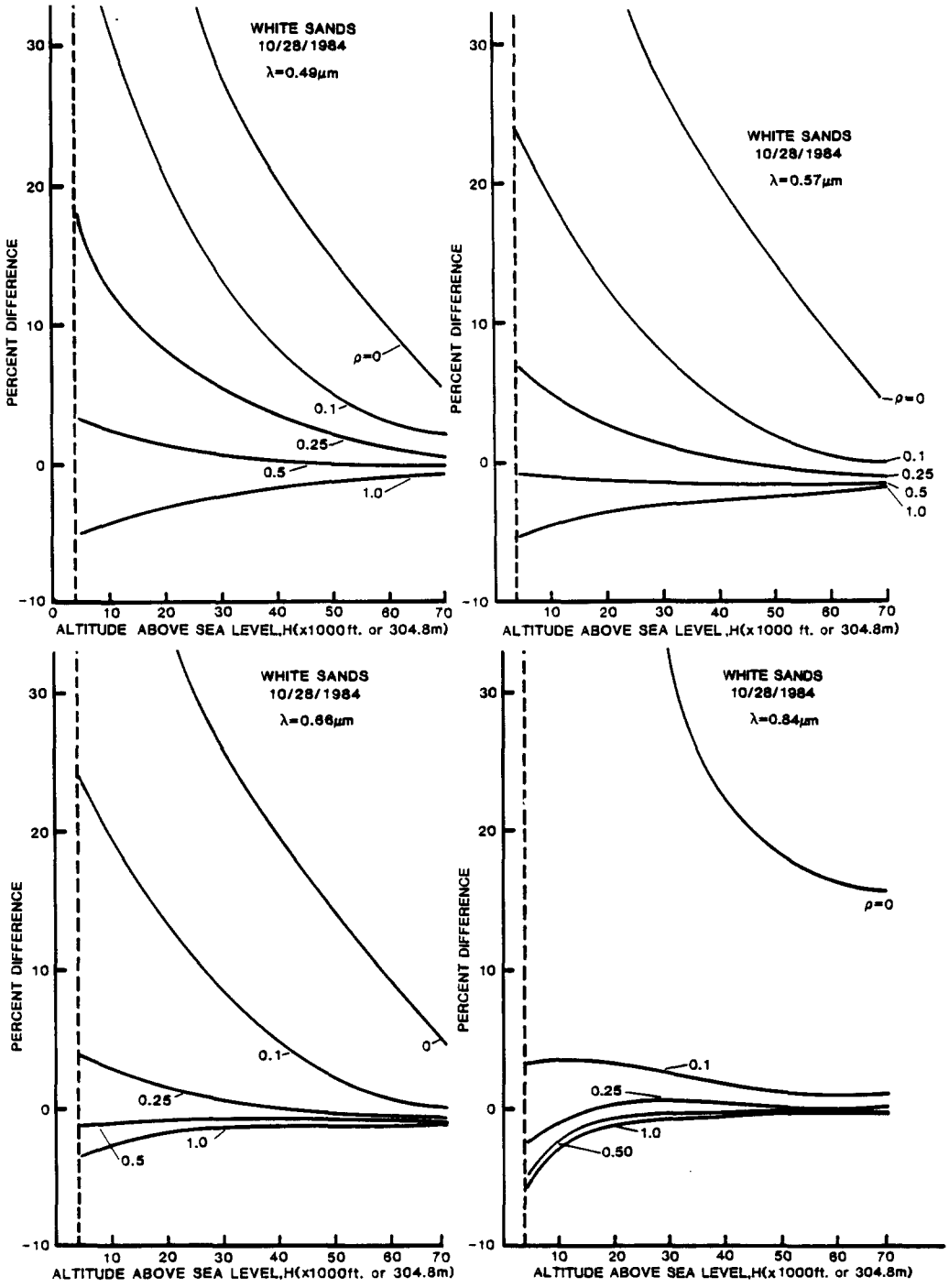

FIGURE 10. Percentage differences between the radiances at the top of the atmosphere and at intermediate altitudes for the White Sands conditions of 28 October 1984; see Table 4.

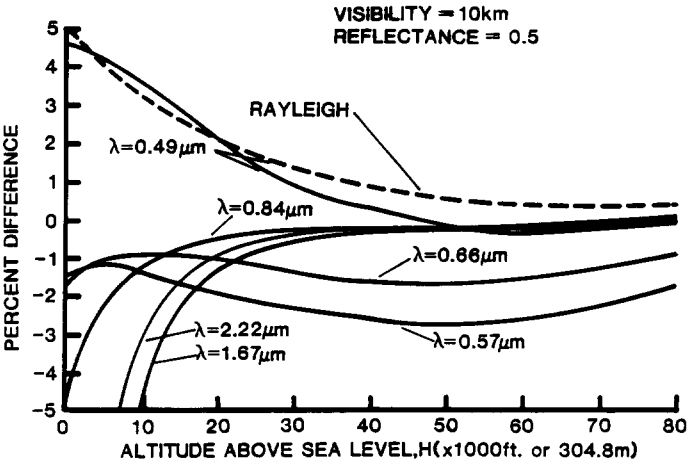

FIGURE 11. Percentage differences between the radiances at the top of the atmosphere and at intermediate altitudes for $\rho = 0.5$ and a visibility of 10 km.

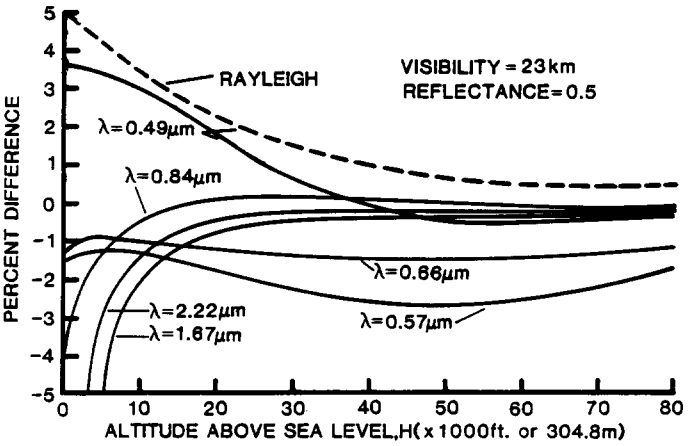

FIGURE 12. Percentage differences between the radiances at the top of the atmosphere and at intermediate altitudes for $\rho = 0.5$ and a visibility of 23 km.

tive differences for altitudes approaching ground level, owing to the heavy aerosol loading in the lower atmosphere. The bowing of the $\lambda = 0.57$ and 0.66 μm curves at intermediate altitudes is due to reduced path radiance from Rayleigh scattering and the presence of ozone absorption at those altitudes. Note that for an altitude of 3000 m and a visibility of 23 km the percentage differences are $+3.0$, -1.4, -0.9, -0.8, -2.3, and -1.6 for wavelengths of 0.49, 0.57, 0.66, 0.84, 1.67, and 2.22 μm, respectively. Furthermore, the percentage differences are less than twice these values for a visibility of 10 km, as can be seen from the remarkable similarity between Figs. 11 and 12.

Conclusion

Satellite multispectral sensors typically exhibit reduced sensivities in flight compared to preflight. In the case of the CZCS, an exponential degradation has been noted that is greater in the short wavelength bands than in the long wavelength bands. The results presented here for the TM visible bands demonstrate the same lower sensitivity in flight than preflight and suggest that there is a tendency for this to be wavelength dependent but to a lesser degree than for CZCS. Also the observation by Hovis et al. (1985) that the decrease in the CZCS response is due entirely to a reduction in the transmittance of the telescope may not hold for the TM. For the TM visible bands, our reflectance-based and radiance-based measurements, taken in conjunction with the internal calibrator results, indicate that the reduction in sensitivity may be due partly to a loss in telescope transmittance and partly to a loss in sensitivity of the filters, detectors, and associated electronics.

For the 12 reflectance-based measurements we have made in the TM visible bands, the RMS variation from the mean as a percentage of the mean is $\pm 1.9\%$ over a 16-month period. For 11 measurements in the IR bands it is $\pm 3.4\%$. The RMS variation for all 23 measurements is $\pm 2.8\%$. (All RMS variations are 1 σ). Whether the higher RMS variation in the IR is because the system response is less stable in the IR than in the visible or because there are inaccuracies in our determination of the effect of water-vapor absorption, or a combination of the two, is hard to ascertain. Sensitivity analyses (Kastner and Slater, 1982; Kastner, 1985) have shown that a large uncertainty (30%) in water-vapor content for mean conditions at White Sands of 0.1 $g\,cm^{-2}\,km^{-1}$ changes the radiance in TM band 5 by only 2%. It seems probable therefore that the observed variations are due mainly to changes in the system's response. Incidentally, we are at a disadvantage with respect to Bands 5 and 7 because an inadequate signal-to-noise ratio prevents our making ground-radiance measurements with the spectropolarimeter from a helicopter in these bands.

A comparison between the counts per unit spectral radiance as determined by our measurements (CODE), the preflight calibration (PRE), and the internal calibrator (IC) in-flight shows excellent agreement between CODE and IC values in the visible but consistently high values for the PRE, and good agreement between the PRE and IC values in the IR but consistently high values for CODE. As pointed out by Markham and Barker (1987), there are significant changes in the output of the IC with temperature of the IC flag in Bands 5 and 7. The IC on TM-4 showed a $\pm 7\%$ oscillatory variation in Bands 5 and 7. This probably also occurs in TM-5 but there are insufficient data to prove this (Barker, 1986a). Thus, although the evidence is not conclusive, there are independent indications that the IC calibrations are less reliable in Bands 5 and 7, and perhaps in Band 4, than in Bands 1, 2, and 3.

The measurement of reflected spectral radiance by a helicopter at 3000 m MSL has been shown experimentally and theoretically to offer a precise alternative procedure to reflectance-based calibration for bands in the visible and near IR. However, when a given calibration method,

such as the reflectance-based method described here, is said to provide results that agree to within ±2.8%, this is an uncertainty in precision and not necessarily in absolute accuracy. The value of a precise, independent second method, which can be used simultaneously with the first, is that when the two agree to within their error budgets, we can become more confident that their precision represents an absolute accuracy. This then is one important reason for making the helicopter radiance-based measurements, and the reason we hope others will continue their independent calibration studies at White Sands.

Having achieved an uncertainty in precision of ±2.8% for our calibrations at White Sands, we plan to refine the measurements and modify the digital counts obtained at White Sands. We expect the most important improvements will be achieved by making sky polarization measurements and reflected-radiance measurements from a helicopter at the time of sensor overflight. The results of the polarization measurements should improve our knowledge of the aerosol size distribution and the real part of the aerosol refractive index. The use of helicopter radiance data with ground reflectance and optical-depth data will permit a comparison of actual and predicted spectral radiances at the helicopter altitude. We anticipate that a change in the imaginary part of the aerosol refractive index, which is used in the radiative-transfer code, will allow the results to be equalized. This seems to be a promising method to determine the effective imaginary part of the refractive index in the vertical air column above the ground site—a quantity that is difficult to measure by other methods and that probably represents the greatest uncertainty in the calibration. We also plan to determine the effect of the low-reflectance area surrounding White Sands on the code-predicted radiance values at the sensor, which assume an infinite surface of uniform reflectance. Finally, there are several TM detector-electronic effects that must be taken into account now that the 3% level of precision has been reached. These include the memory effect, the unequal quantization bin sizes, and other small radiometric errors that may amount, at the most, to three digital counts or about 2% of the radiance level for TM Bands 1–4 at White Sands. Further information on these effects can be found in other papers in this issue and in a special issue of *Photogrammetric Engineering and Remote Sensing* devoted to the Landsat Image Data Quality Assessment program (Markham and Barker, 1985).

We wish to thank the following for their contributions to the satellite calibration program at White Sands while they were graduate students at the Optical Sciences Center, University of Arizona: C. J. Bruegge (née Kastner), B. A. Capron, K. R. Castle, L. J. Lingg, A. L. Phillips, and S. L. Witman. We also wish to thank C. E. Ezra and several foreign scientists for their collaboration: H. Aoki, Che Nianzeng, M. C. Dinguirard, G. Fedosejevs, and P. M. Teillet. The assistance of D. Ferralez, D. Ream and R. K. Savage at the Atmospheric Sciences Laboratory at White Sands Missile Range is also gratefully acknowledged. We wish to thank B. M. Herman for the use of his radiative transfer code, J. A. Reagan for the use of his solar radiometer, and both for useful

discussions. Finally we wish to thank J. L. Barker and V. V. Salomonson for their encouragement and support under NASA Contract NAS5-27382.

References

Aranuvachapun, S. (1983), Variation of atmospheric optical depth for remote sensing radiance calculations, *Remote Sens. Environ.* 13:131–147.

Barker, J. L. (1985a), *Relative Radiometric Calibration of Landsat TM Reflective Bands. Landsat-4 Science Characterization Early Results*, NASA Conf. Pub. 2355, Vol. 3, Part 2, pp. 1–219.

Barker, J. L. (1985b and 1986b), Thematic mapper radiometric and algorithm performance program (TRAPP), communication to the authors.

Barker J. L. (1986a) NASA Goddard Space Flight Center, communication to the authors.

Begni, G., Dinguirard, M. C., Jackson, R. D., and Slater, P. N. (1986), Absolute calibration of the SPOT-1 HRV cameras, SPIE, 660:66–76.

Biggar, S. F., Bruegge, C. J., Capron, B. A., Castle, K. R., Dinguirard, M. C., Holm, R. G., Lingg, L. J., Mao, Y., Palmer, J. M., Phillips, A. L., Slater, P. N., Witman, S. L., Yuan, B., Jackson, R. D., Moran, M. S., and Savage, R. K. (1985), Absolute calibration of remote sensing instruments, in *Proc. Third Int. Colloq. on Spectral Signatures of Objects in Remote Sensings*, Les Arcs, France, ESA SP-127.

Bohren, C. F. and Hoffman, D. R. (1983), *Absorption and Scattering of Light by Small Particles*. Wiley, New York, pp. 279–280.

Castle, K. R., (1985), Absolute radiometric calibration of a spectropolarimeter, PhD dissertation, University of Arizona, 129 pp.

Castle, K. R., Holm, R. G., Kastner, C. J., Palmer, J. M., Slater, P. N., Dinguirard, M., Ezra, C. E., Jackson, R. D., and Savage, R. K. (1984), Inflight absolute radiometric calibration of the Thematic Mapper, *IEEE Trans. Geosci. Remote Sens.* GE-22:251–255.

Dave, J. B. (1969), Scattering of electromagnetic radiation by a large, absorbing sphere, *IBM J. Res. Rev.* (May):302–313.

Elterman, L. (1966) Aerosol measurements in the troposphere and stratosphere, *Appl. Opt.* 5:1769–1776.

Fröhlich, C. (1983), Data on total and spectral irradiance: comments, *Appl. Opt.* 22:3928.

Gordon, H. R. (1981), Reduction of error introduced in the processing of coastal zone color scanner-type imagery resulting from sensor calibration and solar irradiance uncertainty, *Appl. Opt.* 20:207–210.

Gordon, H. R. (1987), Calibration requirements and methodology for remote sensors viewing the ocean in the visible, *Remote Sens. Environ.* 22:103–126.

Gordon, H. R., Clark, D. K., Brown, J. W., Brown, O. B., Evans, R. H., and Broenkow, W. W. (1983a), Phytoplankton pigment concentrations in the Middle Atlantic Bight: Comparison of ship determinations and CZCS estimates, *Appl. Opt.* 22:20–36.

Gordon, H. R., Brown, J. W., Brown, O. B., Evans, R. H., and Clark, D. K., (1983b), Nimbus 7 CZCS: reduction of its radiometric sensitivity with time, *Appl. Opt.* 22:3929–3930.

Herman, B. M., and Browning, S. R. (1975), The effect of aerosols on the earth–atmosphere albedo, *J. Atmos. Sci.* 32:158–165.

Hovis, W. A., Knoll, J. S., and Smith, G. R. (1985), Aircraft measurement for calibration of an orbiting spacecraft sensor, *Appl. Opt.* 24:407–410.

Iqbal, M. (1983), *An Introduction to Solar Radiation*, Academic, New York.

Jackson, R. D., Moran, M. S., Slater, P. N., and Biggar, S. F. (1987), Field calibration of reference reflectance panels, *Remote Sens. Environ.* 22:145–158.

Jennings, S. G., Pinnick, R. G., and Auvermann, H. J. (1978), Effects of particulate complex refractive index and particle size distribution variations on atmospheric extinction and absorption for visible through middle IR wavelengths, *Appl. Opt.* 17:3922–3929.

Junge, C. E. (1963), *Air Chemistry and Radioactivity*, Academic, New York.

Kastner, C. J. (1985), Absolute radiometric calibration of the Landsat Thematic Mapper, PhD dissertation, University of Arizona, 195 pp.

Kastner, C. J., and Slater, P. N. (1982), In-flight radiometric calibration of advanced remote sensing systems, *Proc. SPIE* 356:158–165.

Kneizys, F. X., Shettle, E. P., Gallery, W. O., Chetwynd, Jr., J. H., Abreu, L. W., Selby, J. E. A., Clough, S. A., and Fenn, R. W. (1983), Atmospheric transmittance/radiance: computer code LOWTRAN 6, Report AFGL-TR-83-0187, AFCRL, Bedford, MA.

Koepke, P. (1982), Vicarious satellite calibration in the solar spectral range by means of calculated radiances and its application to Meteosat, *Appl. Opt.* 21:2845–2854.

Markham, B. L., and Barker, J. L., Eds. (1985), Landsat image data quality analysis, *Photogramm. Eng. Remote Sens.* 51 (Special LIDQA issue):1245–1493.

Markham, B. L., and Barker, J. L. (1987), *Remote Sensing Environ.* 22:39–71.

McClatchey, R. A., Fenn, R. W., Selby, J. E. A., Volz, F. E., and Garing, J. S. (1972), Optical properties of the atmosphere, Report AFCRL-72-0497, Environmental Res. Papers, No. 411, AFCRL, Bedford, MA.

Mueller, J. L. (1985), Nimbus-7 CZCS: confirmation of its radiometric sensitivity decay through 1982. *Appl. Opt.* 24:1043–1047.

Palmer, J. M. (1984), Effective bandwidths for Landsat-4 and Landsat D′ Multispectral Scanner and Thematic Mapper subsystem, *IEEE Trans. Geosci. Remote Sens.* GE-22:336–338.

Pearce, W. A. (1977), A study of the effects of the atmosphere on Thematic Mapper observations, Final Report under NASA Contract NAS5-23639.

Robinson, B. F., Bauer, M. E., Dewitt, D. P., Silva, L. F., and Vanderbilt, V. C. (1979), Multiband radiometer for field research, SPIE 196:8–15.

Santer, R. P. (1986), University of Lille, France, communication to the authors.

Shaw, G. E., Reagan, J. A., and Herman, B. M. (1973), Investigation of atmospheric extinction using direct solar radiation measurements made with a multiple wavelength radiometer, *J. Appl. Meterol.* 12:374.

Slater, P. N. (1984), The importance and attainment of absolute radiometric calibration, *Proc. SPIE Critical Rev. Remote Sens.* 475:34–40.

Slater, P. N. (1985), Radiometric considerations in remote sensing, *Proc. IEEE* 73(6):997–1011.

Slater, P. N., Biggar, S. F., Holm, R. G., Jackson, R. D., Mao, Y., Moran, M. S., Palmer, J. M., and Yuan, B. (1986), Absolute radiometric calibration of the Thematic Mapper, SPIE 660:2–8.

Tanré, D., Deroo, C., Dahaut, P., Herman, M., Morcrette, J. J., Perbos, J., and Deschamps, P. Y. (1985), Effets atmospheriques en teledetection-logiciel de simulation du signal satellitaire dans le

spectre solaire, *Proc. Third Int. Colloq. on Spectral Signatures of Objects in Remote Sensing*, ESA SP-247, pp. 315–319.

Teillet, P. M., and Fedosejevs G. (1986), Canada Centre for Remote Sensing, communication to the authors.

Voillier, M. (1982), Radiometric calibration of the Coastal Zone Color Scanner on Nimbus 7: a proposed adjustment, *Appl. Opt.* 21:1142–1145.

Received 10 September 1986; revised 22 December 1986.